Journal of CO_2 Utilization 21 (2017) 562–571

Contents lists available at ScienceDirect

Journal of CO_2 Utilization

journal homepage: www.elsevier.com/locate/jcou

Effect of support nature on the cobalt-catalyzed CO_2 hydrogenation

J. Díez-Ramírez[a,*], P. Sánchez[a], V. Kyriakou[b,c], S. Zafeiratos[d], G.E. Marnellos[c,e,f], M. Konsolakis[g], F. Dorado[a]

[a] Departamento de Ingeniería Química, Facultad de Ciencias y Tecnologías Químicas, Avenida Camilo José Cela 12, 13071 Ciudad Real, Spain
[b] Department of Chemical Engineering, Aristotle University of Thessaloniki, Building E13, GR-54124, Greece
[c] Chemical Process Engineering Research Institute, Chemical Process & Energy Resources Institute, Centre for Research & Technology Hellas, GR-57100 Thermi-Thessaloniki, Greece
[d] Institut de Chimie et Procédés Pour l'Energie, L'Environnement et la Santé (ICPEES), ECPM, UMR 7515 CNRS-Université de Strasbourg, 25, Rue Becquerel, Strasbourg Cedex 02, France
[e] Department of Mechanical Engineering, University of Western Macedonia, GR-50100 Kozani, Greece
[f] Department of Environmental Engineering, University of Western Macedonia, GR-50100 Kozani, Greece
[g] School of Production Engineering and Management, Technical University of Crete, GR-73100 Chania, Crete, Greece

ARTICLE INFO

Keywords:
CO_2 hydrogenation
Methanation
Co-based catalysts

ABSTRACT

CO_2 hydrogenation to value added chemicals/fuels has gained considerable interest, in terms of sustainable energy and environmental mitigation. In this regard, the present work aims to investigate the CO_2 methanation performance of cobalt-based catalysts supported on different metal oxides (M_xO_y: CeO_2, ZrO_2, Gd_2O_3, ZnO) at low temperatures (200–300 °C) and under atmospheric pressure. Various characterization methods, such as N_2 adsorption-desorption at −196 °C, X-ray diffraction (XRD), X-ray photoelectron spectroscopy (XPS) and temperature-programmed reduction (TPR), were employed to correlate the structural and surface properties of the materials with their catalytic activity. The results revealed a significant impact of support nature on the CO_2 hydrogenation performance. The following order, in terms of CH_4 yield (Y_{CH4}), was recorded at 300 °C: Co/CeO_2 (~96%) > Co/ZnO (~54%) > Co/G_2O_3 (~53%) ~ Co/ZrO_2 (~53%). On the basis of the characterization results, the superiority of Co/CeO_2 catalyst can be mainly ascribed to its enhanced reducibility linked to Co-Ceria interactions. Moreover, Co/CeO_2 demonstrated a stable conversion/selectivity performance under subsequent reaction cycles, in contrast to Co/ZnO, which progressively activated under reaction conditions. The latter is related with the modifications induced in elemental chemical states and surface composition of Co/ZnO upon pretreatment in reaction conditions, in contrast to Co/CeO_2 sample where a stable surface performance was observed.

1. Introduction

During the past two centuries, the world's energy demands have considerably increased due to the growing population and industrialization [1,2]. Nowadays, almost 80% of these needs are met by carbon-containing fossil fuels, such as oil, natural gas and coal leading to increasing CO_2 emissions [1–3]. The dependence on fossil fuels is not expected to decline sufficiently in the forthcoming years, while the energy demands are predicted to grow by ca. 35% [1]. On the other hand, the intensive use of fossil fuels is considered responsible for the increase of CO_2 atmospheric concentration by more than 30% in the last 50 years [4]. Carbon dioxide constitutes the major greenhouse gas, contributing to the Earth's global warming effect and to the acidification of the oceans [4].

To efficiently manage the risks associated with global warming, the anthropogenic CO_2 emissions should be limited in order to meet the challenging targets set by the global Paris Agreement and the EU 2030 Framework for climate and energy. Three main routes could be followed toward addressing this issue: i) CO_2 emissions reduction [5], ii) Carbon Capture and Sequestration (CCS) [3,5–8] and iii) CO_2 transformation to value added chemicals or fuels [3,6]. The first approach requires the development of more efficient energy conversion fossil fuel technologies and/or the switching to renewable energy sources (RES). On the other hand, CCS faces some major issues related mainly to the long-term stability of storage locations [3,5–8]. The chemical transformation of CO_2 to useful products is among the most viable strategies, since not only could sustain the atmospheric concentration of CO_2 at acceptable levels but also provides value added chemicals/fuels, such as

* Corresponding author.
E-mail address: Javier.Diez@uclm.es (J. Díez-Ramírez).

http://dx.doi.org/10.1016/j.jcou.2017.08.019
Received 19 May 2017; Received in revised form 25 August 2017; Accepted 27 August 2017
Available online 12 September 2017

methane and methanol [6,9,10].

However, the CO_2 molecule is very stable, requiring an energy demanding, catalyst-aided, process for its activation [11,12]. The most common and sustainable way to activate CO_2 involves its interaction with hydrogen being generated from RES-powered water electrolysis. This particular process could also serve as a promising approach to efficiently store the excess electricity from intermittent renewable sources (solar, wind), which in turn can be transformed *via* CO_2 hydrogenation to fuels, such as methane or methanol [3,11,13–15]. In this regard, the CO_2 hydrogenation constitutes one of the most challenging processes in the field of catalysis [3,11,13–15]. Depending on the catalyst used, a variety of products can be derived, such as methanol [13], methane (Sabatier reaction) [14], higher hydrocarbons [15] and CO [11], according to the following reactions:

$$CO_2(g) + H_2(g) \leftrightarrow CO(g) + H_2O(g), \quad \Delta H_{298} = 41.2\ kJ/mol \quad (1)$$

$$CO_2(g) + 3H_2(g) \leftrightarrow CH_3OH(g) + H_2O(g), \quad \Delta H_{298} = -49.6\ kJ/mol \quad (2)$$

$$CO_2(g) + 4H_2(g) \leftrightarrow CH_4(g) + 2H_2O(g), \quad \Delta H_{298} = -165.0\ kJ/mol \quad (3)$$

$$xCO_2(g) + yH_2(g) \leftrightarrow C_xH_{2y-4x}(g) + 2H_2O(g) \quad (4)$$

In the last few years, a wide variety of materials have been tested as catalysts for the above reactions. Among them, Cu, Pd and Zn have been reported as the most active catalysts for reducing CO_2 to methanol and CO (Reactions (1), (2)) [3,13,16–21], while Ni, Rh and Ru are the most effective for producing hydrocarbons (Reactions (3), (4)) [22–24]. Ni-based catalysts are much cheaper than Ru and Rh, but they suffer from deactivation, due to the sintering of Ni particles and carbon poisoning [*e.g.*,25,26].

On the other hand, cobalt-based catalysts are widely used in Fischer-Tropsch synthesis, since they combine high performance for the hydrogenation of CO to hydrocarbons with a relatively low cost [3]. However, if CO feed is switched to CO_2, then Co-based catalysts are highly active and selective toward the formation of methane (Reaction (3)) [3,27–36]. The latter has been ascribed to the weaker adsorption of CO_2 as compared to CO on the Co surface, leading to lower C/H ratios, which favor the formation of methane instead of higher hydrocarbons (Reaction (4)) [37].

The conversion of CO_2 and the selectivity to CH_4 depends on various parameters, involving among others, the preparation procedure [29,38,39], the metal loading [30,40,41] and the supporting carrier [27,30,40]. Especially, the latter is of crucial importance. It has been well established that the support nature can notably affect the redox and adsorptive properties of the catalyst, through strong metal-support interactions, with important effects on the catalytic performance [14,27,32,42–45]. Suslova et al. [27] showed that apart from the particle size and oxidation state of Co entities, the catalytic activity and selectivity of CO_2 hydrogenation process can be notably affected by the nature of the support. The presence or not of a reducible carrier could modify the local surface structure of Co and consequently, its catalytic behavior [27].

In the light of the above aspects, the present work aims to systematically explore the impact of support nature on the physicochemical properties and the CO_2 hydrogenation activity/stability of Co-based catalysts, at intermediate temperatures (200–300 °C) and under atmospheric pressure. Four metal oxides (CeO_2, ZrO_2, Gd_2O_3, ZnO) of different textural/redox characteristics were employed as supporting materials. The physicochemical properties of the catalysts were evaluated by means of XRD, BET, TPR and XPS techniques to gain insight into possible structure-activity relationships.

Table 1
Textural and structural characteristics of Co/M_xO_y samples.

	Co/Gd_2O_3	Co/ZrO_2	Co/CeO_2	Co/ZnO
Cobalt loading (wt. %)[a]	37.6	41.7	42.3	39.8
Surface area ($m^2\ g^{-1}$)[b]	19	14	29	4.7
Total pore volume ($cm^3\ g^{-1}$)	0.08	0.06	0.11	0.04
Crystallite size of metallic Co after reduction (nm)	n.d.[c] – 31.3[d]	45.9[c] – 34.2[d]	42.2[c] – 27.4[d]	47.3[c] – 40.9[d]
Cobalt dispersion (%)[e]	3.2	2.9	3.6	2.4

[a] Determined by atomic absorption (AA) spectrophotometry.
[b] Determined by the multi-point BET method.
[c] Determined by the Scherrer equation (XRD).
[d] Determined by TEM.
[e] Determined by Eq. (9) using the particle size from TEM.

2. Experimental

2.1. Catalyst preparation

Co-based catalysts were prepared through the wet impregnation method, employing $Co(NO_3)_2{\cdot}6H_2O$ (Sigma Aldrich, 99.999% purity) as precursor compound [46]. For the synthesis of bare oxides (CeO_2, ZrO_2, Gd_2O_3 and ZnO), the appropriate stoichiometric quantities of the corresponding precursor nitrates (> 99% metal purity, Sigma Aldrich) were diluted in distilled water to prepare an aqueous solution. The solution was stirred on a hot plate until water evaporation, followed by drying overnight at 100 °C and calcination at 600 °C for 2 h. The resulting oxides were then added to the aqueous solution of Co nitrate, at the appropriate concentration of the desired loading (40 wt.% Co). This specific loading was dictated from preliminary studies (not included) concerning the impact of metal loading (20–60 wt.%) on the catalytic activity. The solvent was removed *via* heating under continuous stirring and the sample was then dried overnight at 100 °C and calcined at 600 °C for 2 h.

2.2. Catalyst characterization

Cobalt loading was determined by atomic absorption (AA) spectrophotometry on a SPECTRA 220FS analyser. Samples (*ca.* 0.5 g) were treated with 2 mL HCl, 3 mL HF and 2 mL H_2O_2 followed by microwave digestion (523 K).

Surface area/porosity measurements were carried out using a QUADRASORB 3SI sorptometer apparatus with N_2 as the sorbate at 77 K. The samples were outgassed at 523 K under vacuum (5×10^{-3} Torr) for 12 h prior to analysis. Specific surface areas were determined by the multi-point BET method. The total pore volume was evaluated from N_2 uptake at a relative pressure of P/Po = 0.99.

Temperature-programmed reduction (TPR) experiments were conducted in a commercial Micromeritics AutoChem 2950 HP unit with TCD detection. Samples (*ca.* 0.15 g) were loaded into a U-shaped tube and ramped from room temperature to 973 K (10 K min^{-1}), using a reducing gas mixture of 17.5% v/v H_2/Ar (60 $cm^3\ min^{-1}$).

The degree of reduction was calculated according to the following equation:

$$R(\%) = \frac{\text{Actual } H_2 \text{ amount}\left(\frac{mmol}{g}\right)}{\text{Theoretical } H_2 \text{ amount}\left(\frac{mmol}{g}\right)} \quad (5)$$

where the actual amount of H_2 is determined by the quantification of TPR profiles in the low temperature range where the reduction of Co_xO_y is mainly taking place, whereas the theoretical H_2 corresponds to the

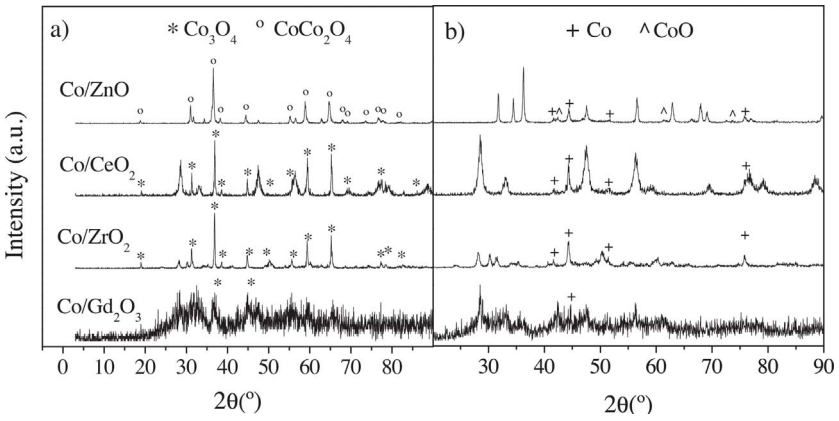

Fig. 1. XRD profiles prior (a) and after (b) the reduction for the different supported catalysts.

stoichiometric amount of H_2 required to completely reduce Co_3O_4 according to (Eq. (6)):

$$Co_3O_4 + 4H_2 \rightarrow 3Co + 4H_2O \quad (6)$$

assuming negligible reduction of oxide carriers in the low temperature range [41].

XRD analyses were conducted with a Philips X'Pert instrument using nickel-filtered Cu-Kα radiation. Samples were scanned at a rate of 0.02° $step^{-1}$ over the range of 5° ≤2θ ≤ 90° (scan time = 2 s $step^{-1}$).

Transmission electron microscopy (TEM) analyses were conducted in a JEOL JEM-4000EX unit with an accelerating voltage of 400 kV. Samples were prepared by ultrasonic dispersion in acetone with a drop of the resulting suspension evaporated onto a holey carbon-supported grid. TEM images were obtained over used samples, *i.e.* over samples subjected to reaction conditions (see below).

The particle size was calculated from TEM images. The mean particle size evaluated as the surface-area weighted diameter ($\bar{d}_s$), and was calculated according to:

$$\bar{d}_s = \frac{\sum_i n_i d_i^3}{\sum_i n_i d_i^2} \quad (7)$$

where n_i represents the number of particles with diameter d_i ($\Sigma_i n_i \geq 200$).

The X-ray photoelectron spectroscopy (XPS) measurements were carried out in an ultrahigh vacuum (UHV) spectrometer described elsewhere [47]. Spectra were recorded with a VSW Class WA hemispherical electron analyzer using a monochromated Al Kα X-ray source (1486.6 eV). Survey and high resolution XP spectra were recorded in constant pass energy mode (100 and 44 eV, respectively). An electron flood gun was used to compensate for differential surface charging of insulating samples, while the C 1s of adventitious carbon at 285 eV was used as a reference of the binding energy scale. The surface atomic ratio was calculated using the integrated XPS peak areas, normalized to the atomic sensitivity factors.

2.3. Catalytic evaluation studies

Experiments were carried out in a tubular quartz reactor (45 cm length and 1 cm diameter). The catalyst (0.6 g), with a particle size in the range of 250–500 μm and without dilution, was placed on a fritted quartz plate located at the end of the reactor. The temperature of the catalyst was measured with a K-type thermocouple (Thermocoax) placed inside the catalyst bed. The entire reactor was placed in a furnace (Lenton) equipped with a temperature-programmed controller. Reaction gases were Praxair certified standards of CO_2 (99.999% purity), H_2 (99.999% purity) and N_2 (99.999% purity). The gas flows were controlled by a set of calibrated mass flowmeters (Brooks 5850 E and 5850 S).

The experimental procedure followed for the activity and stability tests is described in the following. Prior to the reaction, all samples were reduced *in situ* in a hydrogen stream (10% vol) diluted with nitrogen at a flow rate of 25 cm^3 min^{-1}. The temperature was increased at a heating rate of 10 °C min^{-1} up to 450 °C, and kept constant for 2 h. Then the sample was purged in N_2 flow and the temperature decreased to 200 °C. The reaction was then carried out at atmospheric pressure in the temperature range of 200–300 °C. The feed contained a CO_2/H_2 mixture (CO_2/H_2 molar ratio = 1/9) with P_{CO2} = 10 kPa, P_{H2} = 90 kPa and a total flowrate of 75 cm^3/min. Gases were monitored by a micro gas chromatograph (Varian CP-4900). Product's selectivity (S_i) was calculated as shown in Eq. (8) considering the following chemical species: CO, CH_4, C_2H_6, C_3H_8 and CH_3OH. It should be noted that under the present reaction conditions, the selectivity to higher hydrocarbons was always lower than 5%.

$$S_i(\%) = \frac{n_i x r_i}{\sum_i n_i x r_i} x100 \quad (8)$$

where n_i is the number of carbon molecules and r_i the formation rate of product i, respectively.

To gain insight into the intrinsic reactivity of Co/M_xO_y catalysts, the turnover frequency (TOF_i, min^{-1}) for each product (i) was also calculated according to the equation:

$$TOF_i(min^{-1}) = \frac{r_i(mol\ min^{-1} g_{Co}^{-1}) \times A_{Co}(g_{Co}\ mol^{-1})}{D_{Co}/100} \quad (9)$$

where r_i is the formation rate of product i, A_{Co} is the atomic mass of Co (58.93 g_{Co} mol^{-1}), and D_{Co} is the Co dispersion. The dispersion of cobalt, D_{Co}, was calculated based on the Co particle size obtained by TEM analysis, according to the following equation [48]:

$$D_{Co}(\%) = \frac{6 \times A_{Co} \times n_S}{\rho_{Co} \times N_{Av} \times d_{Co}} \times 100 \quad (10)$$

where n_s is the number of Co atoms at the surface per unit area (1.51×10^{19} at m^{-2}), ρ_{Co} is the density of cobalt (8900×10^3 g m^{-3}), N_{Av} is the Avogadro's number (6.023×10^{23} at mol^{-1}) and d_{Co} is the average Co particle diameter determined by TEM.

Motivated by the progressive activation under reaction conditions and in order to examine the stability performance, indicated samples were imposed to successive heating/cooling cycles during reaction. In particular, after the completion of the 1st cycle of catalytic evaluation measurements, the sample was cooled down to room temperature under N_2 flow, remaining at this stage for 12 h. Then, the catalytic behavior was again explored (2nd cycle) by increasing the temperature up to 300 °C. The following nomenclature was used throughout the text in relation to the state of catalysts: fresh (as prepared samples calcined at 600 °C for 2 h), reduced (fresh catalysts imposed to reduction at 450 °C for 2 h under 10% v/v H_2), used (after the completion of the 2nd cycle of catalytic activity measurements).

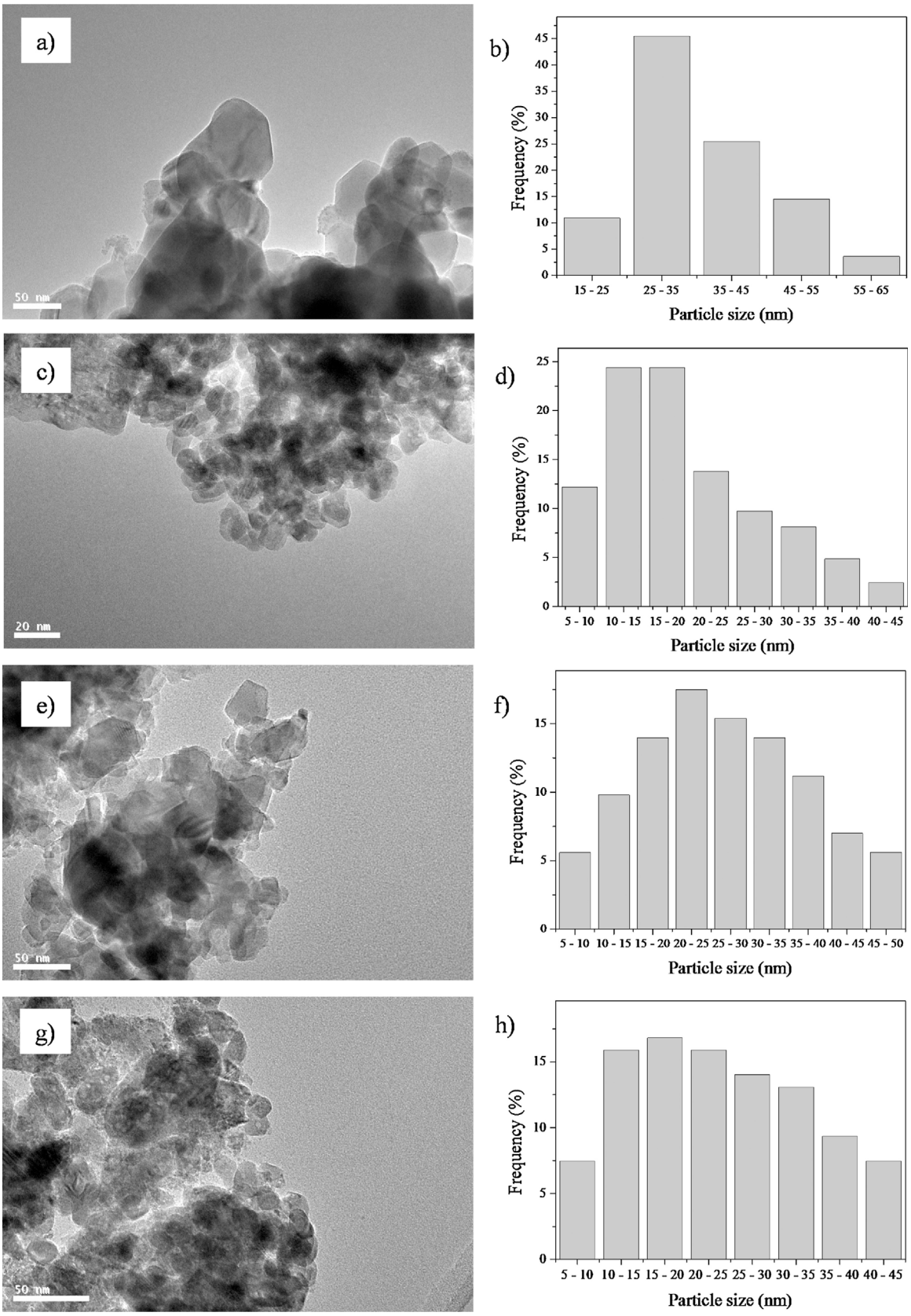

Fig. 2. TEM images and metal particle distribution of (a, b) Co/ZnO, (c, d) Co/CeO_2, (e, f) Co/ZrO_2, and (g, h) Co/Gd_2O_3 used samples.

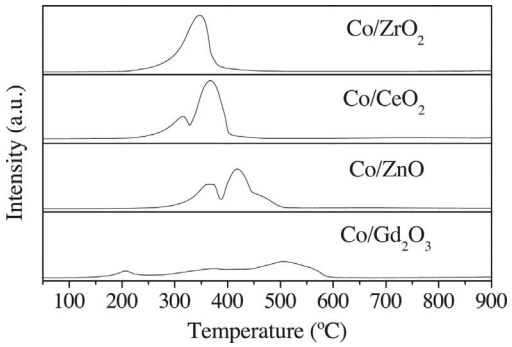

Fig. 3. TPR profiles of Co/M_xO_y samples.

3. Results and discussion

3.1. Textural and structural characteristics

Table 1 summarizes the main textural characteristics of as prepared (fresh) Co-based samples, in terms of surface area and total pore volume. It is evident that the Co/CeO_2 sample possesses the highest BET area ($29\ m^2\ g^{-1}$), followed by Co/Gd_2O_3 ($19\ m^2\ g^{-1}$) > Co/ZrO_2 ($14\ m^2\ g^{-1}$) > Co/ZnO ($4.7\ m^2\ g^{-1}$). These differences could be realized by taking into account the different structural characteristics of the supporting carriers, as will be discussed below.

Fig. 1a shows the XRD patterns of as prepared (fresh) Co-based samples. To gain insight into the impact of reduction pretreatment, the corresponding XRD patterns of reduced samples are comparatively shown in Fig. 1b. In Table 1, the mean crystallite size of metallic cobalt phase as determined by the Scherrer equation and TEM images is also presented. Cobalt particle size and dispersion values are in agreement with BET area results: the higher the particle size, the lower the surface area.

Regarding the fresh samples, the cobalt oxide (Co_3O_4, JCPDS 78-1970) was the predominant phase of cobalt entities detected in Co/CeO_2 and Co/ZrO_2 samples. This inorganic compound is a mixed oxide with cobalt valences of +2 and +3. It generally adopts the normal spinel structure with Co^{2+} ions in tetrahedral interstices and Co^{3+} ions in the octahedral interstices of the cubic close-packed lattice of oxide anions [49]. However, for the Co/ZnO catalyst, the binary spinel of Co_3O_4 was found. It is listed as $CoCo_2O_4$ (JCPDS 80-1545), to distinguish among the double and triple positively charged ions at the tetrahedral site [50]. The other peaks that appear in the diffractograms were related to the different supports. Zinc oxide (JCPDS 80-0075) showed a hexagonal system and cerium oxide a cubic system (JCPDS 81-0792). For zirconium oxide, there were reflections peaks of two different systems: monoclinic system (JCPDS 07-0343) along with the tetragonal system (JCPDS 88-1007). Finally, Co/Gd_2O_3 catalyst showed an amorphous structure, hindering the precise identification of different phases, although the presence of Co_3O_4 may be sensed.

A comparison between the XRD patterns of fresh (Fig. 1a) and reduced (Fig. 1b) samples reveals various new reflections at 41.78°, 44.36°, 47.30° and 51.28°, which are attributed to the cubic metallic cobalt (JCPDS 01-1259). The Co/ZnO catalyst showed some peaks of cobalt oxide (CoO) with cubic structure (JCPDS 78-0431), demonstrating an incomplete reduction of cobalt oxide under the present reduction conditions. This could be assigned to the formation of a hardly reducible $ZnCo_2O_4$ phase, which it is possible to be formed at a moderate cobalt content [51]. This compound shows a cubic structure (JCPDS 23-1390) with peaks similar to those of $CoCo_2O_4$. Therefore, its presence cannot be discarded. On the other hand, there were no oxide peaks in the Co/CeO_2 and Co/ZrO_2 samples, suggesting their complete reduction. Finally, as commented above, Co/Gd_2O_3 XRD spectrum is unclear and hence it is impossible to deny or confirm the existence of oxides or other compounds.

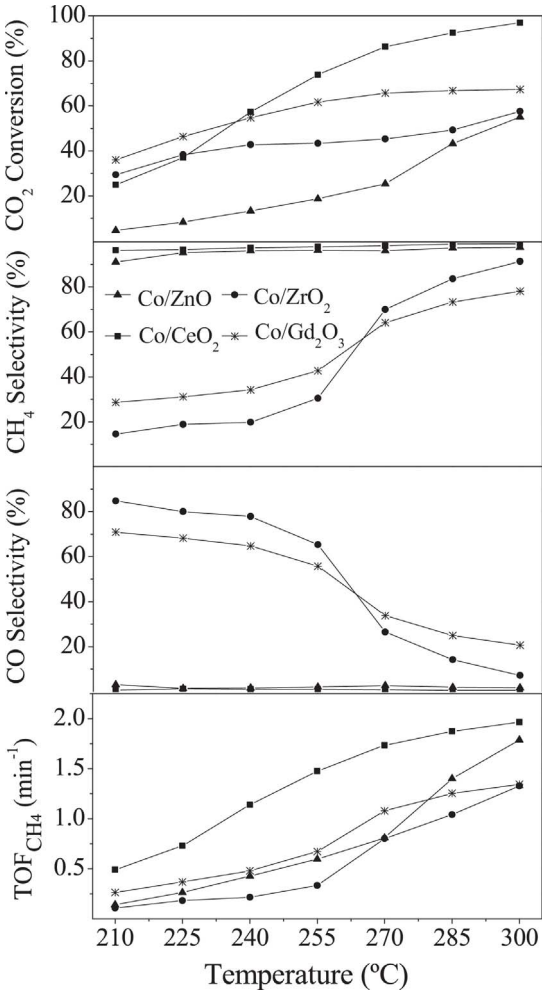

Fig. 4. Conversion of CO_2, selectivity toward CH_4 and CO and TOF of CH_4 for the Co/M_xO_y catalysts during CO_2 hydrogenation. Reaction conditions: CO_2/H_2 = 1/9 and W/F = 0.008 g min cm^{-3}.

TEM images are shown in Fig. 2. All catalysts exhibit a Gaussian distribution of particle size, with the maximum following the order of: Co/ZnO > Co/ZrO_2 > Co/Gd_2O_3 > Co/CeO_2. Thus, the Co/ZnO sample showed the highest particle size and Co/CeO_2 exhibited the

Table 2
TPR characteristics of Co/M_xO_y samples.

Sample	Main peaks (°C)			Co_3O_4 content (mmol/g)[a]	H_2 consumption (mmol/g)[b]	H_2 theoretical (mmol/g)	Reduction degree (%)
Co/Gd_2O_3	199	364	497	2.1	7.4	8.5	87
Co/ZrO_2	341	–	–	2.4	7.9	9.4	84
Co/CeO_2	310	362	–	2.4	8.7	9.6	91
Co/ZnO	367	415	–	2.3	7.1	9.0	79

[a] Determined by atomic absorption (AA) spectrophotometry.
[b] Determined by the quantification of H_2-TPR profiles.

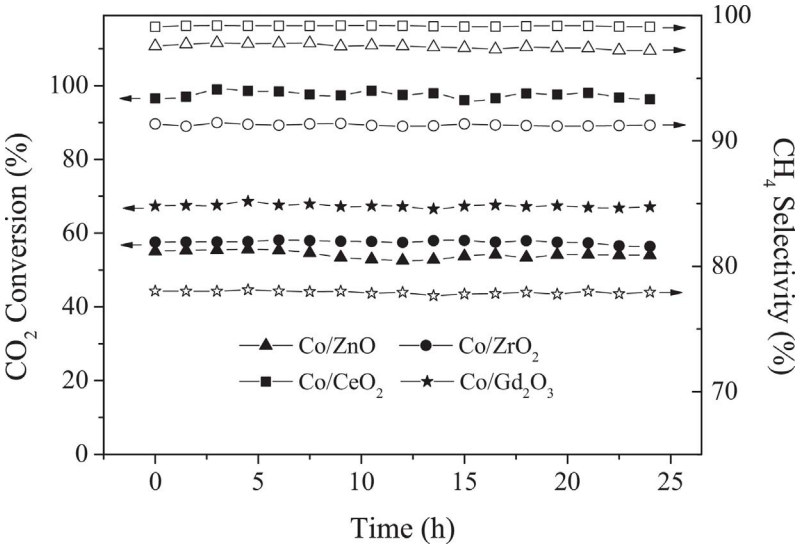

Fig. 5. Catalytic stability of the Co/M_xO_y catalysts during CO_2 hydrogenation. Reaction conditions: 300 °C, CO_2/H_2 = 1/9 and W/F = 0.008 g min cm^{-3}.

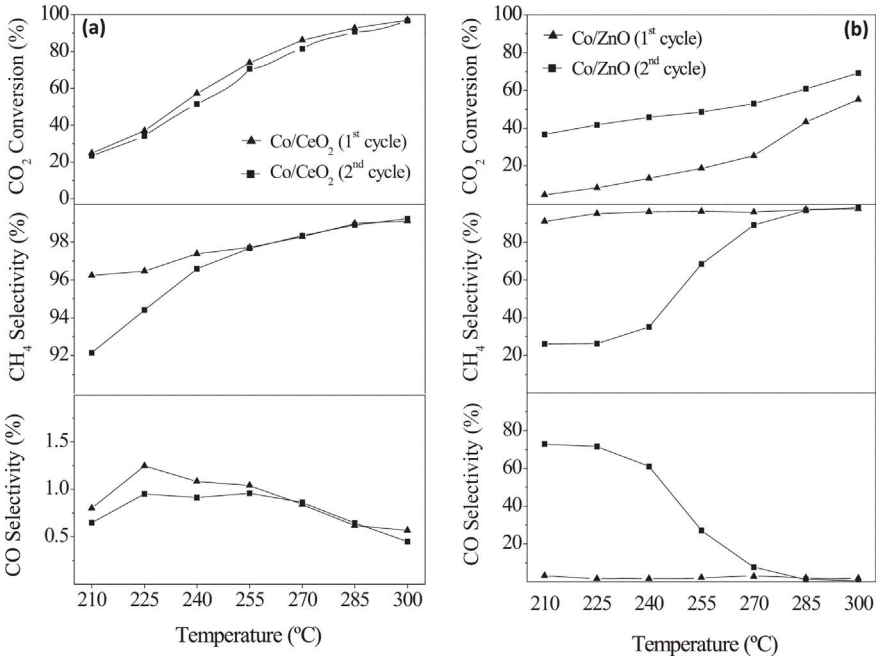

Fig. 6. Conversion and selectivity performance of Co/CeO_2 (a) and Co/ZnO (b) in two subsequent catalytic evaluation tests: catalytic assessment upon temperature increase (1st cycle) followed by cool down to room temperature under N_2 flow (12 h), and reevaluation (2nd cycle). Reaction conditions: CO_2/H_2 = 1/9 and W/F = 0.008 g min cm^{-3}.

lowest, confirming the difference in the BET area between the samples.

3.2. Redox properties

Fig. 3 depicts the TPR profiles of the Co/M_xO_y samples. In Table 2, the main TPR peaks are summarized. The Co/ZrO_2 catalyst exhibited only one reduction peak at 341 °C, probably due to the superimposition of the successive reduction processes of Co^{+3} to Co^{+2} and Co^{+2} to Co^0. For the Co/ZnO catalyst, two reduction peaks were observed, located, however, at higher temperatures as compared to Co/CeO_2. These peaks could be ascribed to the stepwise reduction of cobalt oxide entities with different interaction with the support as well as to the possible contribution of support reduction. Finally, the Co/Gd_2O_3 catalyst showed a wide reduction profile consisting of three broad peaks. This can be attributed to the complex metal-support interactions and support porous structure, resulting in differently reducible cobalt species [44,52].

To gain insight into the impact of support nature on the reducibility of Co-based samples, the amount of H_2 consumption (mmol g^{-1}) was also estimated from the quantification of TPR profiles (Table 2). The reduction degree of Co-based samples, *i.e.*, the ratio of the actual H_2 consumption to the theoretical amount of H_2 required for the complete reduction of Co_3O_4 in each sample, follows the order: Co/CeO_2 (91%) > Co/Gd_2O_3 (87%) > Co/ZrO_2 (84%) > Co/ZnO (79%). The lowest reduction degree of Co/ZnO catalyst is in agreement with the appearance of cobalt oxide phases in the XRD patterns of reduced samples (Fig. 1). As explained above, the unreduced cobalt oxide could be due to a hardly reducible $ZnCo_2O_4$ phase formed during the calcination of the Co/ZnO catalyst. This phase could be also responsible for the reduction temperature shift to higher values for this catalyst [51]. This compound can be reduced in two steps, *i.e.*, $ZnCo_2O_4$ to CoO followed by CoO to Co [53–55].

3.3. Catalytic evaluation studies

The impact of support nature on the CO_2 hydrogenation performance of Co/M_xO_y samples, in terms of CO_2 conversion, selectivity and TOF_{CH4}, is shown in Fig. 4. Significant differences, both in the CO_2 conversion and the selectivity to various products, were observed

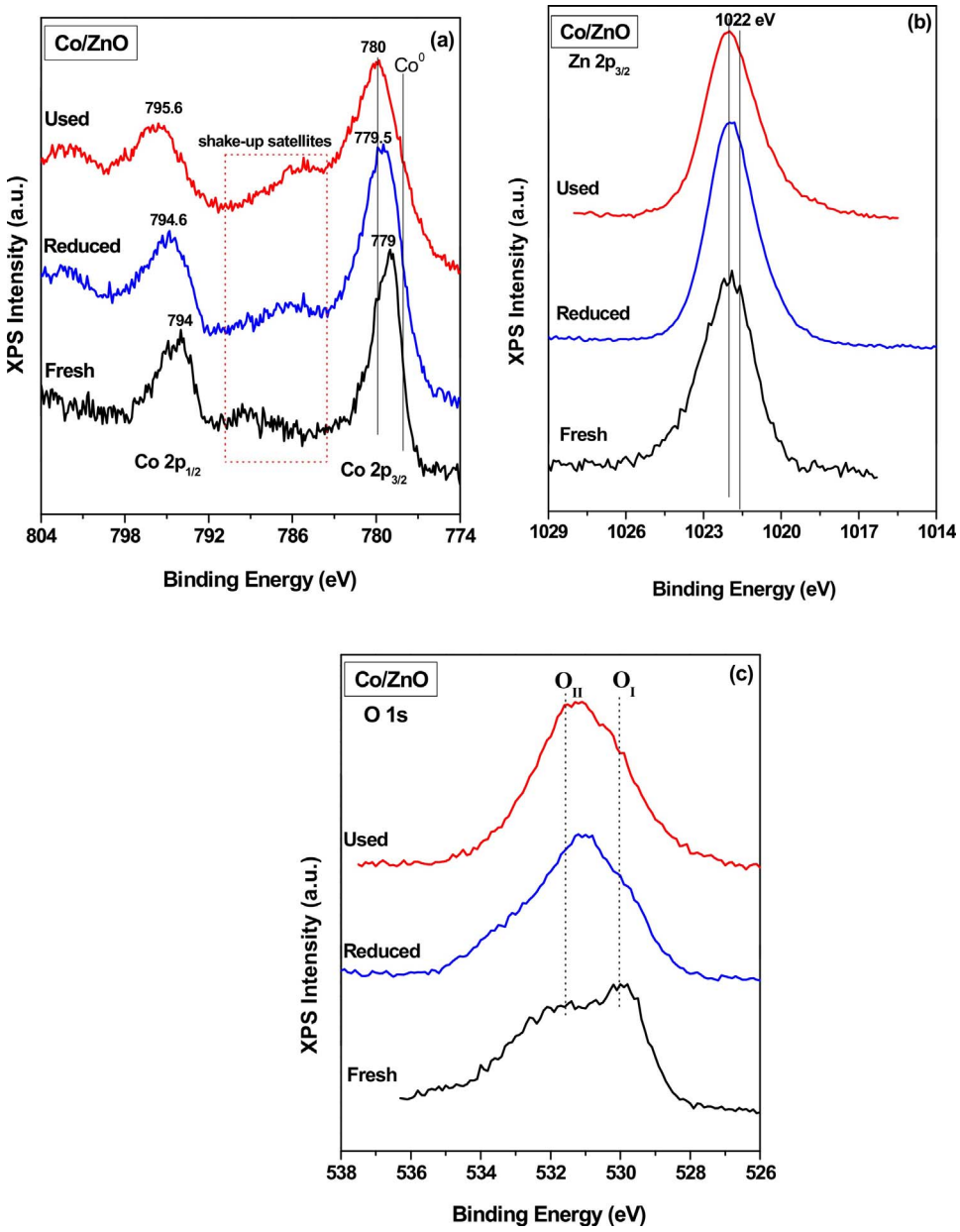

Fig. 7. XPS spectra of Co/ZnO sample imposed to different pre-treatment in the Co 2p (a), Zn 2p (b) and O 1s (c) region.

amongst the Co/M_xO_y samples, implying the key-role of the support on the CO_2 hydrogenation activity. In particular, the Co/CeO_2 sample demonstrated the optimum performance in terms of CO_2 conversion (97.0% at 300 °C), followed by Co/Gd_2O_3 (67.4%) > Co/ZrO_2 (57.6%) > Co/ZnO (55.1%). It is worth noticing that the conversion performance follows the same trend as the reduction degree of Co/M_xO_y catalysts (Table 2), implying a possible reducibility-activity correlation, as will be further discussed below. Regarding the selectivity to various products, both Co/CeO_2 and Co/ZnO are highly selective to CH_4 (> 90%) at all temperatures examined (200–300 °C). On the other hand, the selectivity towards CH_4 of Co/ZrO_2 and Co/Gd_2O_3 follows a similar sigmoidal trend; progressively increasing with the temperature at the expense of CO. At 300 °C the following CH_4 yields (the product of CO_2 conversion and methane selectivity) are obtained: Co/CeO_2 (~96%) > Co/ZnO (~54%) > Co/G_2O_3 (~53%) ~ Co/ZrO_2 (~53%). Higher hydrocarbons (ethane and propane) as well as methanol were also observed at the lower temperatures examined, but with selectivities lower than 5%. Interestingly the TOF values for methane formation follow the same trend with the achieved CH_4 yields. In particular, at 300 °C, the following activity order, in terms of TOF values were recorded: Co/CeO_2 (2.0 min^{-1}) > Co/ZnO (1.8 min^{-1}) > Co/Gd_2O_3 (1.3 min^{-1}) ~ Co/ZrO_2 (1.3 min^{-1}). The temperature of 300 °C was selected to carry out a 24-h stability test for all catalysts (Fig. 5). All samples exhibited stable performance, with insignificant variations in the values of CO_2 conversion and CH_4 selectivity.

Motivated by the incomplete reduction of Co/ZnO under H_2 flow (Fig. 1, Table 2) as well as by its inferior conversion performance compared to CeO_2-based samples, the catalytic behavior of these two samples was further assessed through successive heating/cooling reaction cycles (see Section 2) to reveal the impact of pre-treatment under reaction conditions (CO_2/H_2 mixture) on the methanation performance.

Fig. 6 shows the conversion and selectivity performance of Co/CeO_2 and Co/ZnO during the two subsequent cycles. It is evident that both CO_2 conversion and selectivity to CH_4 and CO were not altered in the case of Co/CeO_2 sample, implying the establishment of a stable performance upon the completion of the 1st cycle. In total contrast, the CO_2 conversion of Co/ZnO was notably increased in the 2nd cycle, indicating a progressive activation under reaction conditions. At the same time, the selectivity to CH_4 was decreased at lower temperatures

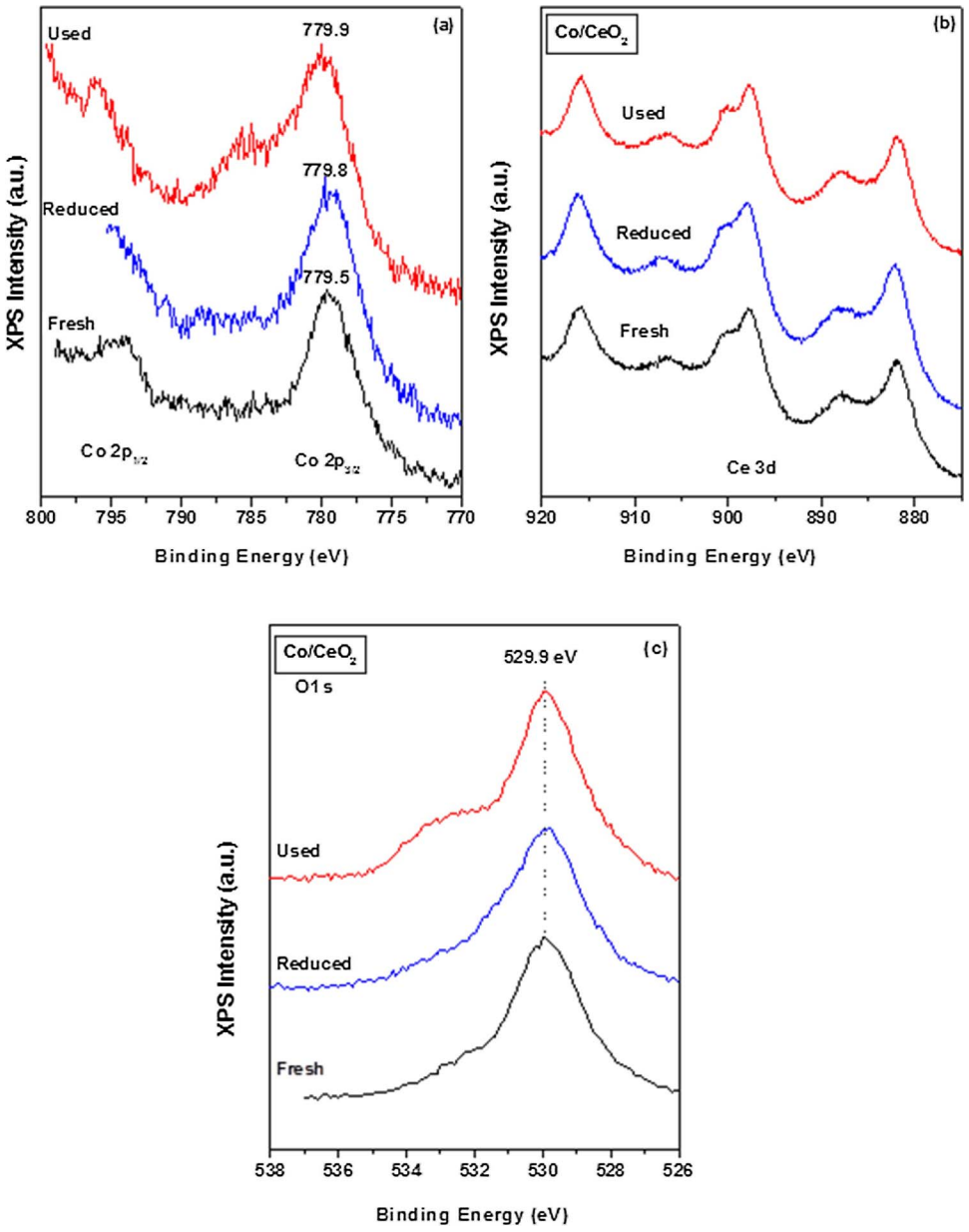

Fig. 8. XPS spectra of Co/CeO_2 sample imposed to different pre-treatment in the Co 2p (a), Ce 3d (b) and O 1s (c) region.

during the 2nd cycle, in contrast to 1st cycle where it remains almost stable (> 90%) in the whole temperature range. It should be also noticed that the catalytic behavior of the used Co/ZnO is practically the same to the one obtained with the fresh Co/Gd_2O_3 and Co/ZrO_2 samples (Fig. 4); at low temperatures the CO_2 conversion to CO is favored at the expense of CH_4, whereas at high temperatures the opposite is true. Thus, this behavior seems to be predominant for the metallic cobalt active phase under atmospheric pressure. The latter is further confirmed by the XPS findings (see below) which imply an increased population of reduced Co species on the surface of the used Co/ZnO catalyst.

However, a different behavior was observed for Co/CeO_2 catalyst. At low temperatures and high CO_2 conversion conditions, the selectivity to CH_4 is favored. This could be understood taking into account the mechanism of the CO_2 hydrogenation reaction in relation to the specific characteristics of the ceria support. On the one hand, it is likely that CO_2 hydrogenation to methane proceeds through CO_2 adsorption and dissociation into CO and O ad-species and the subsequent hydrogenation of adsorbed CO [56]. CO_2 adsorption takes place preferably on the metal-support interface, while CO_2 dissociation proceeds on the active metal surface. On the other hand, the presence of hydroxyl (-OH) groups on partially reduced ceria favors the formation of formate species, which are considered as active intermediates toward methane formation [56–58]. The latter could explain the superiority of cobalt-ceria catalyst to convert the chemisorbed CO to methane in the temperature range explored. In a similar manner Ni/CeO_2 catalysts showed the highest CH_4 yield at low temperatures compared to α-Al_2O_3-, TiO_2- and MgO-based catalysts, which was attributed to the high surface coverage of ceria by CO_2-derived species in conjunction to its enhanced redox properties [59,60]. In view of the above, Ceria-based mixed oxides have been recently denoted as one of the most promising carriers for CO_2 methanation due to their unique redox/surface properties [60,61].

3.4. Surface chemistry elucidation

To gain further insight into the impact of pretreatment procedure (fresh, reduced, used) on the catalytic performance of Co/CeO_2 and Co/ZnO samples, XPS analysis was next carried out. Valuable insights in relation to elemental chemical states and surface composition can be

Table 3
Surface atomic ratios in Co/ZnO and Co/CeO_2 samples imposed to a different pretreatment.

Atomic ratio	Sample state		
	Fresh	Reduced	Used
	Co/CeO_2		
Co/O	0.09	0.08	0.09
Ce/O	0.32	0.34	0.31
Co/Ce	0.28	0.23	0.29
	Co/ZnO		
Co/O	0.18	0.20	0.33
Zn/O	0.18	0.31	0.27
Co/Zn	1.00	0.64	1.23

obtained. Fig. 7 depicts the Co 2p, Zn 2p and O 1 s XPS spectra for fresh, reduced and used Co/ZnO sample. The Co 2p spectrum of the fresh sample is characterized by a main peak at ca. 779 eV, accompanied by a low intensity satellite and a spin-orbit doublet $Co2p_{1/2}$–$Co2p_{3/2}$ of about 15 eV. These features point to the formation of Co^{3+} species in Co_3O_4-like phase [41,62,63]. Reduction pretreatment results in an increased intensity of satellite peak at ca.786 eV as well as in an upward shift of Co 2p peaks by about 0.5 eV. These findings suggest the partial reduction of Co^{3+} to Co^{2+} in octahedral sites [64–68]. Interestingly, after reaction conditions (used catalysts) an even higher upward shift (by ca. 1.0 eV) is observed, implying a more efficient reduction of cobalt oxide species. The latter is further verified by the increase of spin-orbit doublet $Co2p_{1/2}$–$Co2p_{3/2}$ to 15.6 eV, as compared to 15.0 and 15.1 eV over fresh and reduced samples, respectively [69].

At the same time the Zn $2p_{3/2}$ peaks shown in Fig. 7b remain practically unaffected upon the different treatments. It is known that the Zn 2p doublet is not particularly sensitive to modifications of the chemical environment around Zn atoms [70], and even in cases of mixed $Zn_{1-x}Co_xO$ oxides fails to give measurable binding energy shifts as compared to ZnO [71].

Fig. 7c depicts the corresponding O 1s XPS spectra for fresh, reduced and used Co/ZnO sample. The fresh sample is characterized by two main components at ca. 530 and 531.5 eV. The low binding energy (BE) peak (O_I) at 530 eV can be ascribed to the lattice oxygen, whereas the one at high BE (O_{II}) at 531.5 eV is related to adsorbed oxygen species, hydroxyl/carbonate groups and oxygen vacancies [72]. The high BE band gains in intensity on reduced and especially on used samples, implying an increase on the relative population of particularly active surface oxygen species and/or oxygen vacancies at the expense of lattice oxygen [69].

The present results reveal a dynamic change of Co/ZnO surface under reduction (H_2) and particularly under reaction (CO_2/H_2) conditions, which may be accounted for the differences obtained between the 1st and 2nd catalytic cycle (Fig. 6). No complete reduction is achieved by the H_2 reduction procedure prior the 1st cycle catalytic evaluation, in complete agreement with the XRD and TPR results, which imply the existence of partially oxidized CoO phase after the reduction treatment. However, a progressive reduction can be achieved under reaction conditions (1st cycle test), resulting in a progressive activation and thus enhanced catalytic performance during the 2nd cycle.

The corresponding XPS spectra for Co/CeO_2 sample are depicted in Fig. 8. The Ce 3d and O 1s spectra slightly affected by the pretreatment, whereas the Co 2p spectrum follows a similar behavior to that obtained for Co/ZnO sample (Fig. 7). These findings could be considered responsible for the stable performance of Co/CeO_2 sample upon the subsequent cycles (Fig. 6), as further demonstrated below.

In Table 3, the surface content of all chemical elements was calculated using the corresponding core level peaks, properly normalized to the photoemission cross section and assuming a homogeneous distribution arrangement model. It is evident that minor changes in the surface content occur in the Co/CeO_2 samples upon the different treatments. However, the Co/O and Co/Zn atomic ratios are considerably increased over the used Co/ZnO sample, as compared to the reduced one, implying an enrichment of catalyst surface to Co species. Hence, Co/ZnO pretreatment under reaction conditions results in an increased population of reduced Co species on the catalyst surface, which could be accounted for the differences observed between the 1st and the 2nd cycle of catalytic measurements. In view of this fact, it was revealed by means of ambient pressure XPS that the active phase of Co_3O_4 oxide during the CO_2 hydrogenation to CH_4 is metallic cobalt [73].

4. Conclusions

The CO_2 hydrogenation process was investigated on Co/M_xO_y (M: Ce, Zr, Gd and Zn) catalysts at temperatures between 200 and 300 °C and under atmospheric pressure. The results revealed the superiority of Co/CeO_2 catalyst, which exhibited an up to 100% conversion of CO_2 to methane. In terms of methane production yield, the following order was found: Co/CeO_2 > Co/ZnO > Co/ZrO_2 > Co/Gd_2O_3. The improved catalytic performance of Co/CeO_2 sample could be mainly ascribed to its superior reducibility linked to Co-Ceria interactions. Moreover, Co/CeO_2 catalyst demonstrated a stable performance in terms of CO_2 conversion and CH_4 selectivity upon subsequent reaction cycles. In contrast, Co/ZnO was progressively activated under reaction conditions due to the enrichment of catalyst surface to metallic cobalt.

Acknowledgments

The authors would like to thank the Ministerio de Economía y Competitividad (project PCIN-2013-183) and the Spanish government (grant FPU13/00727) for their financial support. The authors also thank the General Secretariat of Research and Technology of Greece (13CAPITA-13-8A), for funding of this work in the context of the project "CO_2 and H_2O toward methanol synthesis at atmospheric pressure in co-ionic electrochemical membrane reactors", ERA-NET, 7th FP.

References

[1] C. Ruhl, BP global energy outlook 2030, Vopr. Econ. 5 (2013).
[2] E.V. Kondratenko, G. Mul, J. Baltrusaitis, G.O. Larrazábal, J. Pérez-Ramírez, Status and perspectives of CO_2 conversion into fuels and chemicals by catalytic, photocatalytic and electrocatalytic processes, Energy Environ. Sci. 6 (2013) 3112–3135.
[3] W. Wang, S. Wang, X. Ma, J. Gong, Recent advances in catalytic hydrogenation of carbon dioxide, Chem. Soc. Rev. 40 (2011) 3703–3727.
[4] P.T. Ed. Dlugokencky, NOAA/ESRL (www.esrl.noaa.gov/gmd/ccgg/trends/).
[5] H. Yang, Z. Xu, M. Fan, R. Gupta, R.B. Slimane, A.E. Bland, I. Wright, Progress in carbon dioxide separation and capture: a review, J. Environ. Sci. 20 (2008) 14–27.
[6] M. Mikkelsen, M. Jorgensen, F.C. Krebs, The teraton challenge. A review of fixation and transformation of carbon dioxide, Energy Environ. Sci. 3 (2010) 43–81.
[7] R.M. Cuéllar-Franca, A. Azapagic, Carbon capture, storage and utilisation technologies: a critical analysis and comparison of their life cycle environmental impacts, J. CO_2 Util. 9 (2015) 82–102.
[8] A.J. Hunt, E.H.K. Sin, R. Marriott, J.H. Clark, Generation, capture, and utilization of industrial carbon dioxide, ChemSusChem 3 (2010) 306–322.
[9] G. Férey, C. Serre, T. Devic, G. Maurin, H. Jobic, P.L. Llewellyn, G. De Weireld, A. Vimont, M. Daturi, J.S. Chang, Why hybrid porous solids capture greenhouse gases? Chem. Soc. Rev. 40 (2011) 550–562.
[10] C. Song, Global challenges and strategies for control conversion and utilization of CO_2 for sustainable development involving energy, catalysis, adsorption and chemical processing, Catal. Today 115 (2006) 2–32.
[11] X. Xiaoding, J.A. Moulijn, Mitigation of CO_2 by chemical conversion: plausible chemical reactions and promising products, Energy Fuels 10 (1996) 305–325.
[12] B. Hu, C. Guild, S.L. Suib, Thermal, electrochemical, and photochemical conversion of CO_2 to fuels and value-added products, J. CO_2 Util. 1 (2013) 18–27.
[13] S.G. Jadhav, P.D. Vaidya, B.M. Bhanage, J.B. Joshi, Catalytic carbon dioxide hydrogenation to methanol: a review of recent studies, Chem. Eng. Res. Des. 92 (2014) 2557–2567.
[14] X. Su, J. Xu, B. Liang, H. Duan, B. Hou, Y. Huang, Catalytic carbon dioxide hydrogenation to methane: a review of recent studies, J. Energy Chem. 25 (2016) 553–565.
[15] S. Saeidi, N.A.S. Amin, M.R. Rahimpour, Hydrogenation of CO_2 to value-added products—a review and potential future developments, J. CO_2 Util. 5 (2014) 66–81.
[16] A. Bansode, A. Urakawa, Towards full one-pass conversion of carbon dioxide to

methanol and methanol-derived products, J. Catal. 309 (2014) 66–70.
[17] J. Díez-Ramírez, F. Dorado, A.R. de la Osa, J.L. Valverde, P. Sánchez, Hydrogenation of CO_2 to methanol at atmospheric pressure over Cu/ZnO catalysts: influence of the calcination, reduction, and metal loading, Ind. Eng. Chem. 56 (2017) 1979–1987.
[18]. K.P. Kuhl, E.R. Cave, D.N. Abram, T.F. Jaramillo, New insights into the electrochemical reduction of carbon dioxide on metallic copper surfaces, Energy Environ. Sci. 5 (2012) 7050–7059.
[19] K.C. Waugh, Methanol synthesis, Catal. Lett. 142 (2012) 1153–1166.
[20] J. Díez-Ramírez, J.L. Valverde, P. Sánchez, F. Dorado, CO_2 hydrogenation to methanol at atmospheric pressure: influence of the preparation method of Pd/ZnO catalysts, Catal. Lett. 146 (2016) 373–382.
[21] J. Díez-Ramírez, P. Sánchez, A. Rodríguez-Gómez, J.L. Valverde, F. Dorado, Carbon nanofiber-based palladium/zinc catalysts for the hydrogenation of carbon dioxide to methanol at atmospheric pressure, Ind. Eng. Chem. Res. 55 (2016) 3556–3567.
[22] J. Gao, Q. Liu, F. Gu, B. Liu, Z. Zhong, F. Su, Recent advances in methanation catalysts for the production of synthetic natural gas, RSC Adv. 5 (2015) 22759–22776.
[23] M.A.A. Aziz, A.A. Jalil, S. Triwahyono, A. Ahmad, CO_2 methanation over heterogeneous catalysts: recent progress and future prospects, Green Chem. 17 (2015) 2647–2663.
[24] E. Zağli, J.L. Falconer, Carbon dioxide adsorption and methanation on ruthenium, J. Catal. 69 (1981) 1–8.
[25] M.R. Prairie, A. Renken, J.G. Highfield, K. Ravindranathan Thampi, M. Grätzel, A fourier transform infrared spectroscopic study of CO_2 methanation on supported ruthenium, J. Catal. 129 (1991) 130–144.
[26] D. Wierzbicki, R. Debek, M. Motak, T. Grzybek, M.E. Gálvez, P. Da Costa, Novel Ni-La-hydrotalcite derived catalysts for CO_2 methanation, Catal. Commun. 83 (2016) 5–8.
[27] E.V. Suslova, S.A. Chernyak, A.V. Egorov, S.V. Savilov, V.V. Lunin, CO_2 hydrogenation over cobalt-containing catalysts, Kinet. Catal. 56 (2015) 646–654.
[28] M.K. Gnanamani, G. Jacobs, H.H. Hamdeh, W.D. Shafer, F. Liu, S.D. Hopps, G.A. Thomas, B.H. Davis, Hydrogenation of carbon dioxide over Co-Fe bimetallic catalysts, ACS Catal. 6 (2016) 913–927.
[29] T. Das, S. Sengupta, G. Deo, Effect of calcination temperature during the synthesis of Co/Al_2O_3 catalyst used for the hydrogenation of CO_2, React. Kinet. Mech. Catal. 110 (2013) 147–162.
[30] T. Das, G. Deo, Effects of metal loading and support for supported cobalt catalyst, Catal. Today 198 (2012) 116–124.
[31] W.A.W.A. Bakar, R. Ali, A.A.A. Kadir, S.J.M. Rosid, N.S. Mohammad, Catalytic methanation reaction over alumina supported cobalt oxide doped noble metal oxides for the purification of simulated natural gas, Ranliao Huaxue Xuebao/J. Fuel Chem. Technol. 40 (2012) 822–830.
[32] N. Srisawad, W. Chaitree, O. Mekasuwandumrong, A. Shotipruk, B. Jongsomjit, J. Panpranot, CO_2 hydrogenation over Co/Al_2O_3 catalysts prepared via a solid-state reaction of fine gibbsite and cobalt precursors, React. Kinet. Mech. Catal. 107 (2012) 179–188.
[33] G. Zhou, T. Wu, H. Xie, X. Zheng, Effects of structure on the carbon dioxide methanation performance of Co-based catalysts, Int. J. Hydrogen Energy 38 (2013) 10012–10018.
[34] R. Razzaq, C. Li, M. Usman, K. Suzuki, S. Zhang, A highly active and stable Co_4N/γ-Al_2O_3 catalyst for CO and CO_2 methanation to produce synthetic natural gas (SNG), Chem. Eng. J. 262 (2015) 1090–1098.
[35] V. Iablokov, S.K. Beaumont, S. Alayoglu, V.V. Pushkarev, C. Specht, J. Gao, A.P. Alivisatos, N. Kruse, G.A. Somorjai, Size-controlled model Co nanoparticle catalysts for CO_2 hydrogenation: synthesis, characterization, and catalytic reactions, Nano Lett. 12 (2012) 3091–3096.
[36] J. Janlamool, P. Praserthdam, B. Jongsomjit, Ti-Si composite oxide-supported cobalt catalysts for CO_2 hydrogenation, J. Nat. Gas Chem. 20 (2011) 558–564.
[37] C.G. Visconti, L. Lietti, E. Tronconi, P. Forzatti, R. Zennaro, E. Finocchio, Fischer-Tropsch synthesis on a Co/Al_2O_3 catalyst with CO_2 containing syngas, Appl. Catal. A: Gen. 355 (2009) 61–68.
[38] Y. Liu, H. Wu, L. Jia, Z. Fu, J. Chen, D. Li, D. Yin, Y. Sun, Effect of the calcination temperature on the catalyst performance of ZrO_2-supported cobalt for Fischer-Tropsch synthesis, Adv. Mater. Res. 347–353 (2012) 3788–3793.
[39] K. Takanabe, K. Nagaoka, K. Nariai, K.-i. Aika, Influence of reduction temperature on the catalytic behavior of Co/TiO_2 catalysts for CH_4/CO_2 reforming and its relation with titania bulk crystal structure, J. Catal. 230 (2005) 75–85.
[40] J.G. Choi, H.K. Rhee, S.H. Moon, IR, TPR, and TPD study of supported cobalt catalysts-effects of metal loading and support materials, Korean J. Chem. Eng. 1 (1984) 159–164.
[41] M. Konsolakis, M. Sgourakis, S.A.C. Carabineiro, Surface and redox properties of cobalt-ceria binary oxides: on the effect of Co content and pretreatment conditions, Appl. Surf. Sci. 341 (2015) 48–54.
[42] B. Jongsomjit, J. Panpranot, J.G. Goodwin Jr., Co-support compound formation in alumina-supported cobalt catalysts, J. Catal. 204 (2001) 98–109.
[43] I. Puskas, T.H. Fleisch, P.R. Full, J.A. Kaduk, C.L. Marshall, B.L. Meyers, Novel aspects of the physical chemistry of Co/SiO_2 Fischer-Tropsch catalyst preparations. The chemistry of cobalt silicate formation during catalyst preparation or hydrogenation, Appl. Catal. A: Gen. 311 (2006) 146–154.
[44] W. Chu, P.A. Chernavskii, L. Gengembre, G.A. Pankina, P. Fongarland, A.Y. Khodakov, Cobalt species in promoted cobalt alumina-supported Fischer-Tropsch catalysts, J. Catal. 252 (2007) 215–230.
[45] M. Konsolakis, The role of copper-ceria interactions in catalysis science: recent theoretical and experimental advances, Appl. Catal. B: Environ. 198 (2016) 49–66.
[46] A. Al-Musa, M. Al-Saleh, Z.C. Ioakeimidis, M. Ouzounidou, I.V. Yentekakis, M. Konsolakis, G.E. Marnellos, Hydrogen production by iso-octane steam reforming over Cu catalysts supported on rare earth oxides (REOs), Int. J. Hydrogen Energy 39 (2014) 1350–1363.
[47] W. Luo, S. Zafeiratos, Tuning morphology and redox properties of cobalt particles supported on oxides by an in between graphene layer, J. Phys. Chem. C 120 (2016) 14130–14139.
[48] A. Borodziński, M. Bonarowska, Relation between crystallite size and dispersion onsupported metal catalysts, Langmuir 13 (1997) 5613–5620.
[49] N.N. Greenwood, A. Earnshaw, Chemistry of the Elements, 2nd edition, (1997).
[50] M. Bahmani, B. Vasheghani Farahani, S. Sahebdelfar, Preparation of high performance nano-sized $Cu/ZnO/Al_2O_3$ methanol synthesis catalyst via aluminum hydrous oxide sol, Appl. Catal. A: Gen. 520 (2016) 178–187.
[51] V. Rekha, C. Sumana, S.P. Douglas, N. Lingaiah, Understanding the role of Co in Co-ZnO mixed oxide catalysts for the selective hydrogenolysis of glycerol, Appl. Catal. A: Gen. 491 (2015) 156–162.
[52] R. Ladera, F.J. Pérez-Alonso, J.M. González-Carballo, M. Ojeda, S. Rojas, J.L.G. Fierro, Catalytic valorization of CO_2 via methanol synthesis with Ga-promoted Cu-ZnO-ZrO_2 catalysts, Appl. Catal. B: Environ. 142–143 (2013) 241–248.
[53] Y. Zhang, D. Wei, S. Hammache, J.G. Goodwin Jr., Effect of water vapor on the reduction of Ru-promoted Co/Al_2O_3, J. Catal. 188 (1999) 281–290.
[54] N.N. Madikizela-Mnqanqeni, N.J. Coville, The effect of cobalt and zinc precursors on Co (10%)/Zn (x%)/TiO2 (x = 0,5) Fischer-Tropsch catalysts, J. Mol. Catal. A: Chem. 225 (2005) 137–142.
[55] M. Haneda, Y. Kintaichi, N. Bion, H. Hamada, Alkali metal-doped cobalt oxide catalysts for NO decomposition, Appl. Catal. B: Environ. 46 (2003) 473–482.
[56] S. Rönsch, J. Schneider, S. Matthischke, M. Schlüter, M. Götz, J. Lefebvre, P. Prabhakaran, S. Bajohr, Review on methanation—from fundamentals to current projects, Fuel 166 (2016) 276–296.
[57] B. Ernst, L. Hilaire, A. Kiennemann, Effects of highly dispersed ceria addition on reductibility, activity and hydrocarbon chain growth of a Co/SiO_2 Fischer-Tropsch catalyst, Catal. Today 50 (1999) 413–427.
[58] C. Li, Y. Sakata, T. Arai, K. Domen, K. Maruya, T. Onishi, Adsorption of carbon monoxide and carbon dioxide on cerium oxide studied by Fourier-transform infrared spectroscopy. Part 2. Formation of formate species on partially reduced CeO_2 at room temperature, J. Chem. Soc. Faraday Trans. 1 85 (1989) 1451–1461.
[59] S. Tada, T. Shimizu, H. Kameyama, T. Haneda, R. Kikuchi, Int. J. Hydrogen Energy 37 (2012) 5527.
[60] M.A.A. Aziz, A.A. Jalil, S. Triwahyono, A. Ahmadab, CO_2 methanation over heterogeneous catalysts: recent progress and future prospects, Green Chem. 17 (2015) 2647.
[61] X. Su, J. Xu, B. Liang, H. Duan, B. Hou, Y. Huang, Catalytic carbon dioxide hydrogenation to methane: a review of recent studies, J. Energy Chem. 25 (2016) 553.
[62] M. Konsolakis, Z. Ioakeimidis, Surface/structure functionalization of copper-based catalysts by metal-support and/or metal–metal interactions, Appl. Surf. Sci. 320 (2014) 244–255.
[63] J.H. Kim, X-ray photoelectron spectroscopy analysis of $(Ln_{1-x}Sr_x)$ CoO_{3-8} (Ln: Pr, Nd and Sm), Appl. Surf. Sci. 258 (2011) 350–355.
[64] M. Kang, M.W. Song, C.H. Lee, Catalytic carbon monoxide oxidation over CoO_x/CeO_2 composite catalysts, Appl. Catal. A: Gen. 251 (2003) 143–156.
[65] L.F. Liotta, G. Di Carlo, G. Pantaleo, A.M. Venezia, G. Deganello, Co_3O_4/CeO_2 composite oxides for methane emissions abatement: relationship between Co_3O_4-CeO_2 interaction and catalytic activity, Appl. Catal. B: Environ. 66 (2006) 217–227.
[66] P. Gawade, B. Bayram, A.M.C. Alexander, U.S. Ozkan, Preferential oxidation of CO (PROX) over CoO_x/CeO_2 in hydrogen-rich streams: effect of cobalt loading, Appl. Catal. B: Environ. 128 (2012) 21–30.
[67] L.E. Gómez, A.V. Boix, E.E. Miró, Co/ZrO_2, Co/CeO_2 and MnCoCe structured catalysts for COPrOx, Catal. Today 216 (2013) 246–253.
[68] J.P. Bonnelle, J. Grimblot, A. D'Huysser, Influence de la polarisation des liaisons sur les spectres esca des oxydes de cobalt, J. Electron. Spectrosc. Relat. Phenom. 7 (1975) 151–162.
[69] N.L. Tarwal, K.V. Gurav, T. Prem Kumar, Y.K. Jeong, H.S. Shim, I.Y. Kim, J.H. Kim, J.H. Jang, P.S. Patil, Structure, X-ray photoelectron spectroscopy and photoluminescence investigations of the spray deposited cobalt doped ZnO thin films, J. Anal. Appl. Pyrolysis 106 (2014) 26–32.
[70] C. Ton-That, M.R. Phillips, M. Foley, S.J. Moody, A.P.J. Stampfl, Surface electronic properties of ZnO nanoparticles, Appl. Phys. Lett. 92 (2008).
[71] S. Turczyniak, W. Luo, V. Papaefthimiou, N.S. Ramgir, M. Haevecker, A. Machocki, S. Zafeiratos, A comparative ambient pressure X-ray photoelectron and absorption spectroscopy study of various cobalt-based catalysts in reactive atmospheres, Top. Catal. 59 (2016) 532–542.
[72] M. Konsolakis, Z. Ioakimidis, T. Kraia, G.E. Marnellos, Hydrogen production by ethanol steam reforming (ESR) over CeO_2 supported transition metal (Fe, Co, Ni, Cu) catalysts: insight into the structure-activity relationship, Catalysts 6 (2016).
[73] Y. Zhu, S. Zhang, Y. Ye, X. Zhang, L. Wang, W. Zhu, F. Cheng, F. Tao, Catalytic conversion of carbon dioxide to methane on ruthenium-cobalt bimetallic nanocatalysts and correlation between surface chemistry of catalysts under reaction conditions and catalytic performances, ACS Catal. 2 (2012) 2403–2408.